Controlling silica nanoparticle properties for biomedical applications through surface modification†

Sébastien Legrand,[a] Amélie Catheline,[a] Lucy Kind,[b] Edwin C. Constable,[b] Catherine E. Housecroft,[b] Lukas Landmann,[c] Petra Banse,[c] Uwe Pieles[a] and Amina Wirth-Heller*[a]

Received (in Montpellier, France) 3rd December 2007, Accepted 21st February 2008
First published as an Advance Article on the web 5th March 2008
DOI: 10.1039/b718668a

A study of the intracellular uptake of silica nanoparticles by dog kidney cells (MCDK II) is presented, and their endocytic pathway is elucidated using confocal fluorescence.

Core–shell silica nanoparticles[1] are attractive candidates as containers for modular drug delivery systems.[2] Chemical functionalisation of the surface allows the nanoparticles to be derivatised with a wide variety of functional groups, which can be used for the subsequent attachment of biomarkers[3] or bio-motives[4] for imbuing biocompatibility[5] or immobilisation on surfaces.[6] We are currently interested in the use of core–shell silica nanoparticles as drug delivery systems, and in this Letter we describe methods for controlling the size and aggregation properties, and demonstrate their efficient uptake into living cells.

A number of publications have reported the use of $[Ru(bpy)_3]^{2+}$ salts as luminophores for the facile visualisation of silica nanoparticles *in vivo* and *in vitro*.[7] This luminescent ruthenium complex is a convenient marker, allowing the use of confocal microscopy to localise nanoparticles in various media. We adopted the water-in-oil microemulsion methodology[8] for the preparation of luminescent silica nanoshells incorporating $[Ru(bpy)_3]Cl_2$ ($Ru@SiO_2$). Initially, we determined the factors controlling nanoparticle size and the influence of the luminophore. Different proportions of water or a 1.34 mM aqueous solution of $[Ru(bpy)_3]Cl_2$ were added to n-hexanol–Triton X100–cyclohexane (1 : 2 : 48.5); upon vigorous stirring, the sheering forces generate aqueous nanodroplets in the non-aqueous phase that are stabilized by the surfactant. The proportion of water or aqueous solution added controls the size of the nanodroplets, and ultimately the size of the nanoparticles. In prototype experiments, this microemulsion was treated with tetraethyl orthosilicate (TEOS) followed by aqueous ammonia (28–30%), leading to rapid hydrolysis of the organosilicate and subsequent formation of spherical silica nanoshells encapsulating water ($W@SiO_2$) or the ruthenium dye ($Ru@SiO_2$).[9] Multi-shell silica nanoparticles could be prepared through further addition of TEOS and ammonia after each 24 h reaction time.[10]

The results of SEM studies of dual-shell nanoparticles (one subsequent treatment with TEOS) are presented in Table 1, entries 1–6. As expected, the ratio of water (Table 1, entries 1–5) or aqueous $[Ru(bpy)_3]Cl_2$ solution (Table 1, entry 6) to surfactant influences the nanoparticle size, with greater W : Triton ratios leading to smaller nanoparticles. A comparison of Table 1, entries 3 and 6 reveals that the replacement of water by the solution of $[Ru(bpy)_3]Cl_2$ has a significant influence on the average size of the nanoparticles obtained, presumably as a result of the lowering of the effective concentration of water by the solute. In the cases of Table 1, entries 3–6, the nanoparticles showed a high degree of monodispersivity, but also a tendency to aggregate (Fig. 1a), although at low water–silicate ratios, only aggregated and polydispersed materials were obtained.

We then systematically changed the surface chemistry of the nanoparticles by the introduction of functionalised silicates in the second shell-growth. The use of TEOS alone gave hydrophilic nanoparticles with surface hydroxyl and Si–O–Si functionalities. It is known[11] that the use of 3-aminopropyltriethoxysilane (APTS) results in the formation of surface aminopropyl functionalities. We found that the most efficient and reproducible functionalisation method for aminopropyl-

Table 1 SEM and FESEM data for dual-shell silica nanoparticles

Entry	W : S[a]	Silicate[b]	Guest[c]	Diameter[g] (std[h])/nm
1	1.7 : 1	TEOS	W	Aggregates
2	3.7 : 1	TEOS	W	Polydisperse
3	5.7 : 1	TEOS	W	120 (0.05)
4	7.7 : 1	TEOS	W	90 (0.08)
5	9.7 : 1	TEOS	W	80 (0.09)
6	5.7 : 1	TEOS	R	190 (0.10)
7	5.7 : 1	TEOS/APTS[d]	W	120–180 (0.12)
8	5.7 : 1	TEOS/APTS[d]	R	200 (0.10)
9	5.7 : 1	TEOS/SPEGS[e]	W	130–140 (0.15)
10	5.7 : 1	TEOS/SPEGS[f]	R	200 (0.10)

[a] Molar ratio of water to surfactant. [b] This refers to the silicate or mixture of silicates added for the growth of the second shell. [c] W = water, R = 1.34 mM $[Ru(bpy)_3]Cl_2$. [d] 1 : 1 TEOS–APTS. [e] 3 : 1 TEOS–SPEGS. [f] 10 : 1 TEOS–SPEGS. [g] Observed in SEM images. [h] Standard deviations.

[a] *University of Applied Sciences Northwestern Switzerland, School of Life Sciences, Institute of Chemistry and Bioanalytics, CH-4132 Muttenz, Switzerland. E-mail: amina.wirth@fhnw.ch; Fax: +41 61 467 44 57; Tel: +41 61 467 42 68*
[b] *Department of Chemistry, Spitalstraße 51, CH4056 Basel, Switzerland*
[c] *Clinical Department of Biomedicine (DKBW), University of Basel, Centre for Biomedicine, CH-4058 Basel, Switzerland*

† Electronic supplementary information (ESI) available: xz and yz optical sections of the cells incubated with $Ru@SiO_2$ nanoparticle. See DOI: 10.1039/b718668a

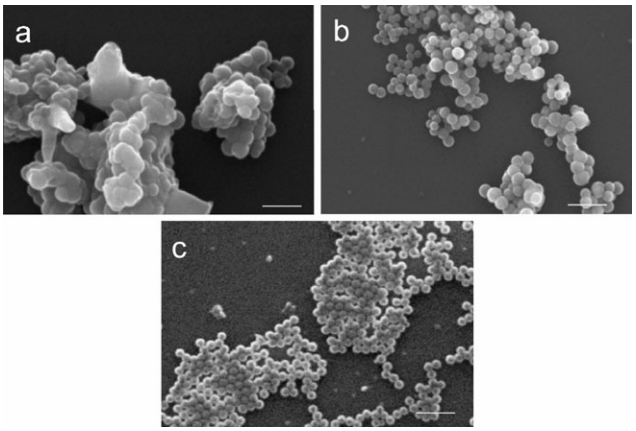

Fig. 1 SEM micrographs of $Ru@SiO_2$ (a) nanoparticles produced without surface modification (Table 1, entry 6), (b) amino-modified particles (Table 1, entry 8) and (c) polyethylene glycol-modified particles (Table 1, entry 10). Samples suspended in water (1 mg ml^{-1}) were deposited on a freshly cleaved mica surface, dried and gold/palladium-coated. SEM experiments were carried out at an accelerating voltage of 20 kV using a StereoScan 360 system (Leica, Cambridge, USA). Scale bars are 1 μm.

derivatised dual-shell nanoparticles involved the growth of the second shell by the co-hydrolysis of a 1 : 1 solution of APTS and TEOS. Nicely monodispersed dual-shell aminopropyl-functionalised nanoparticles were obtained (Table 1, entries 7 and 8; Fig. 1b).

Most notable is the influence of the aminopropyl functionalisation on the dispersion of the nanoparticles, which are seen in the SEM to have minimal aggregation. The FTIR spectra of the aminopropylated nanoparticles exhibited typical amino absorptions at 1627 and 3287 cm^{-1}.

We then considered approaches to developing a biologically benign surface modification of the dual-shell nanoparticles, and decided upon a PEGylated surface. A number of examples of PEGylated silica nanoparticles have been reported,[12] and we describe here a novel strategy for the functionalisation of the outer surface of multi-shell particles. Our strategy was to extend the methodology described above for aminopropyl functionalisation to the preparation of PEGylated derivatives. Furthermore, to preclude the need for monofunctionalised PEG derivatives, we prepared a new bis(silylated)polyethylene glycol SPEGS (Scheme 1).

The new compound, SPEGS, was prepared by the reaction of *O*,*O*′-bis(aminopropyl)-polyethylene glycol 1500 (**1**) with (3-isocyanatopropyl)-triethoxysilane (**2**) in DMSO under argon in the presence of Hünig base (*N*,*N*′-diisopropylethylamine) for 3 h at room temperature (Scheme 2). Removal of the solvent under vacuum gave a white-yellowish gel, which was purged with argon, stored at −20 °C and used without

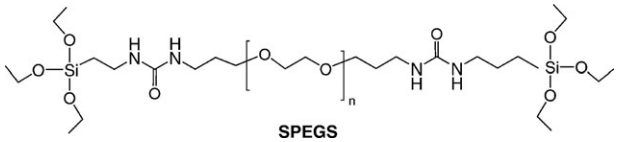

Scheme 1 Chemical structure of the new bis(silylated)polyethylene glycol (SPEGS).

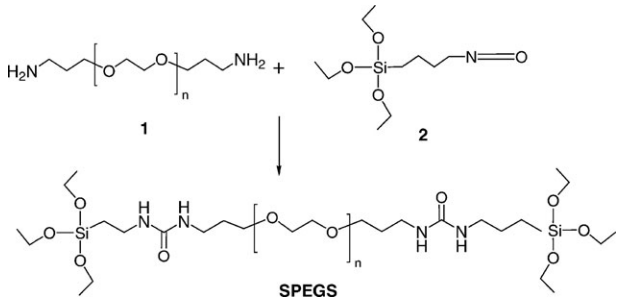

Scheme 2 Synthetic route for the preparation of SPEGS.

further purification. The coupling of the isocyanato groups of **2** with the amino groups of **1** was confirmed by ^1H and ^{13}C NMR spectroscopy.

Dual-shell nanoparticles were prepared with water and $[Ru(bpy)_3]Cl_2$ cores using mixed TEOS and SPEGS for the growth of the second shell (Table 1, entries 9 and 10). The high degree of monodispersivity is seen in Fig. 1c. A critical question is whether the two ends of SPEGS react with the surface of the same nanoparticle or whether they bridge between nanoparticles. Fig. 2 presents a series of SEM and FESEM images of the PEGylated nanoparticles obtained under a variety of conditions. These images have a number of interesting features. Firstly, they have a tendency to form highly ordered two-dimensional arrays on mica, closely resembling a hexagonal close packing (Fig. 2a and c). Fig. 2b shows that a significant number of the nanoparticles are not bridged, and we believe that the bulk of the material is in this form. This is as expected from the synthetic method, where the probability of the growing nanoparticles contacting each other is relatively low. Naturally, we cannot distinguish between species where both ends of the PEG are bound to the nanoparticle and those where only one end is attached. FTIR

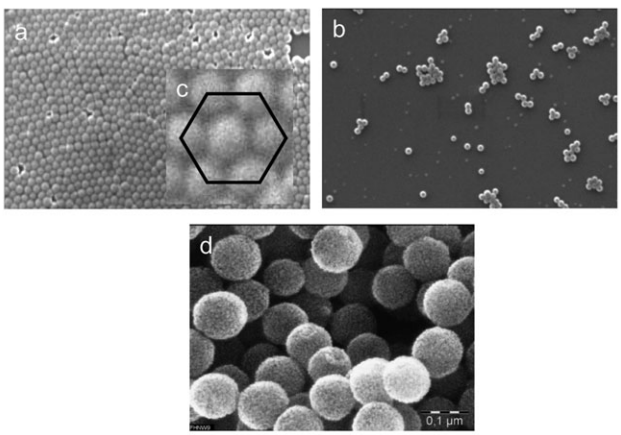

Fig. 2 SEM micrographs of PEGylated dual-shell $Ru@SiO_2$ nanoparticles: (a) SPEGS/TEOS (2 : 10), (b) SPEGS/TEOS (1 : 10), (c) hexagonal packing of silica particles, zoom-in on (b), and (d) high resolution FESEM micrograph of PEGylated dual-shell silica nanoparticles. Suspended samples were deposited on a mica surface, dried and coated with gold/palladium before imaging. FESEM analyses were performed at an accelerating voltage of 20 kV on a field emission scanning electron microscope (FESEM, Zeiss, Supra VP40). Scale bars in (a) and (b) are 1 μm.

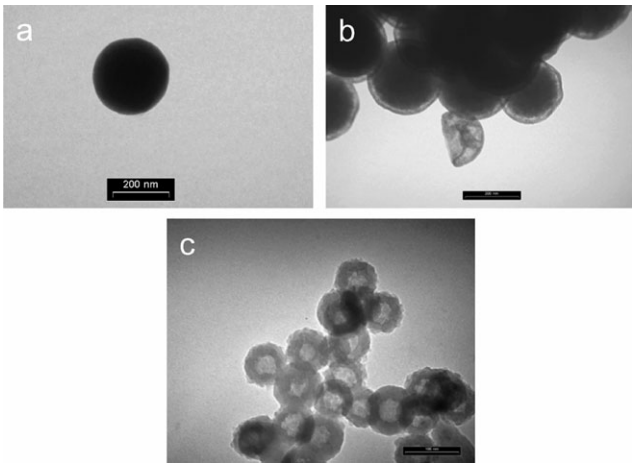

Fig. 3 TEM micrographs of $Ru@SiO_2$ nanoparticles (a) with a non-modified surface, carrying hydroxyl groups, (b) with a PEGylated surface, using a molar ratio of SPEGS–TEOS of about 1 : 10 and (c) with an amino-modified surface, using a molar ratio of APTS–TEOS of 1 : 10. TEM measurements were performed on a Philips CM200. Scale bar is 200 nm in (a) and (b), and 100 nm in (c).

spectra of all the dual-shell silica particles exhibit typical O–Si bands at 1057 cm^{-1}. However, for PEGylated compound, the spectrum showed a small shift in the position of the main peak at 1057 cm^{-1} compared to uncoated particles, indicative of the change in the chemical environment of the silica matrix at the surface.

We then utilised the photophysical properties of $[Ru(bpy)_3]Cl_2$ to further elucidate the influence of the surface chemistry by comparing unmodified (surface OH; Table 1, entry 6), aminopropylated (Table 1, entry 8) and PEGylated (Table 1, entry 10) nanoparticles. The TEM images are presented in Fig. 3, in which the contrast is related to the presence of the heavy metal $[Ru(bpy)_3]Cl_2$ species, allowing us to observe the localisation or delocalisation of the $[Ru(bpy)_3]Cl_2$ luminophore.

In the case of unmodified silica particles, a uniform contrast in the TEM micrograph (Fig. 3a) was obtained, indicating that distribution of the $[Ru(bpy)_3]Cl_2$ dye within the entire particle is homogeneous, whereas a typical core–shell structure was obtained in the case of PEGylated silica particles (Fig. 3b). In the latter case, a clear difference in contrast is observed between the external shell and the particle core, which is indicative of the formation of a hybrid layer around the silica core, which seems to prevent the diffusion of the dye towards the outer shell of the particle. The outer layer thickness is equally uniform and is estimated to be 10–15 nm. Rather surprisingly, in the case of aminopropyl-functionalised particles, the TEM micrograph (Fig. 3c) illustrates dye leaching from the core of the silica particle towards the external shell. We conclude that the PEGylated $Ru@SiO_2$ is suitable for further investigation *in vivo*, as leaching of the luminophore is inhibited.

Finally, we used fluorescence microscopy to image the $Ru@SiO_2$ nanoparticles. When observed at the optimum wavelength (λ_{ex} = 488 nm), a strong fluorescent signal was obtained at the maximum wavelength (λ_{em} = 610 nm). Our

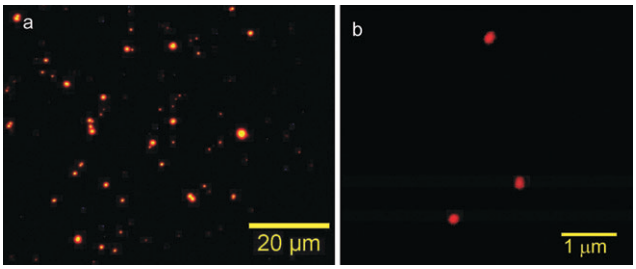

Fig. 4 (a) Fluorescence micrographs of 200 nm $Ru@SiO_2$ silica nanoparticles. (b) Confocal fluorescence. Before imaging with confocal microscopy, the silica particles were first aminopropylated and then immobilised on an epoxide-activated cover slip to ensure their immobilization.

results show that the fluorescence signal of 200 nm-sized nanoparticles increased proportionally with the concentration of the incorporated dye up to a maximum concentration of 1.34 mM, after which a decay in fluorescence intensity was observed, with an asymptotic limit obtained for dye concentrations exceeding 40 mM (data not shown). The fluorescence micrograph in Fig. 4a shows the high fluorescence intensity emitted mainly from large aggregates; single particles can hardly be seen at this resolution. Confocal fluorescence microscopy (Fig. 4b), however, shows a fluorescence signal emitted from three single 200 nm-sized silica particles encapsulating $[Ru(bpy)_3]Cl_2$ at its optimal concentration.

To test the biocompatibility of these modified nanoparticles, we report our initial *in vitro* studies with a dog kidney (MDCK type II) cell line. The intracellular uptake of $Ru@SiO_2$ nanobeads by MDCK II cells was studied using confocal microscopy. Three different samples of silica nanoparticles doped with $[Ru(bpy)_3]Cl_2$ (1.34 mM), with an average diameter of 200 nm, were selected for study. The three samples include unmodified (surface OH; Table 1, entry 6), aminopropylated (Table 1, entry 8) and PEGylated (Table 1, entry 10) nanoparticles. Before use, the silica nanoparticles were dispersed in a mixture of phosphate buffer saline solution (PBS) and Eagles® modified medium (1 : 1) in a concentration of 1 mg ml^{-1}, sonicated and centrifuged in order to spin down the excess particles. MDCK type II cells were seeded on coverslips in a 6-well plate and grown to confluency (2–3 d) in Eagles® modified medium supplemented with 10% canine serum and antibiotics. After washing twice with medium, the cells were incubated for 5 min with the silica nanobeads at a 1 : 4 dilution in medium. After incubation, the cells were washed with PBS to remove excess nanoparticles, and further incubated at 37 °C in a CO_2 incubator in fresh medium for varying periods of time (0, 5, 30 and 60 min). Finally, the incubated cells were fixed for 30 min with 3% of a freshly prepared solution of paraformaldehyde in PBS, and washed 3 times with PBS before immunostaining for the various endocytic compartments. Specimens were analysed by confocal fluorescence microscopy.

To explore the effect of the surface chemistry on endocytosis by cells, different compartment-specific antibodies were used for tracking the endocytotic itinerary of particles using confocal fluorescence microscopy. For this, DAPI (4′,6-diamidino-2-phenylindole dihydrochloride) was used to stain the

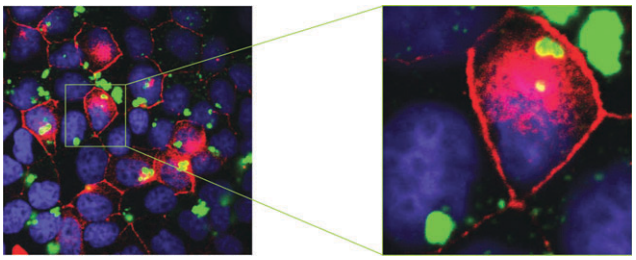

Fig. 5 Confocal fluorescence image of MCDK II cells internalizing unmodified silica nanoparticles after 5 min of incubation (Table 1, entry 6). Channels were rendered artificially; cell boundaries (ZO-1) in red, nuclei in blue and Ru@SiO_2 nanoparticles in green. All images were recorded with an apochromatic 100x/nA 1.4 objective lens. In order to achieve maximum resolution, image stacks were sampled with a voxel size of 50 × 50 × ~130 nm according to the Nyquist theorem.[15]

nucleus, and Cy5-conjugated secondary antibodies were used for visualization of the endocytic compartment-specific primary antibodies. The antibody against a tight junction protein (ZO-1) was used to visualize the cell membrane, EEA1 antibody for the early endosomes, rab7 antibody for the late endosomes and Lamp3 antibody for imaging the lysosomes.[13,14]

The confocal images of MDCK II cells incubated for 5 min with unmodified Ru@SiO_2 nanoparticles are given in Fig. 5. In these micrographs, the nuclei of the whole MDCK cell population are marked in blue DAPI (λ_{ex} = 405 nm, λ_{em} = 420–480 nm), whereas the Cy5-conjugated antibody of tight junction protein (ZO-1) appears in red (λ_{ex} = 633 nm, λ_{em} = 650–710 nm) and the Ru@SiO_2 nanoparticles are green. The images reveal the presence of fluorescent nanoparticles in intracellular domains of the cells but not in cell nuclei. The confocal images also show that the red colour delineates the cell membranes between adjacent cells, and that the green fluorescent particles are present in almost every cell. After confirmation of the cellular uptake of silica particles by MDCK II cells, the different immunostaining assays (described above) were used to elucidate the intracellular fate of unmodified and modified silica nanoparticles over time. The confocal images shown in Fig. 6 demonstrate that, regardless of the surface chemistry, all types of particles were found in the early endosome after only 5 min of incubation, as demonstrated by co-localisation of the green-emitting fluorescence from Ru@SiO_2 particles and the red Cy5-labelled early endosomal marker EEA1 (Fig. 6a–c).

As expected, unmodified particles accumulated more strongly than charged ones. The reason for this difference is not clear and may involve different mechanisms. It is conceivable that negatively-charged particles are repelled by the invaginating membrane, whereas aminopropylated and PEGylated particles prevented the membrane from invaginating by their high affinity.

As the time increases to 10–30 min, only a minor co-localisation of Ru@SiO_2 nanoparticles was observed with Cy5-labelled antibodies against late endosomal protein rab7 (Fig. 7a) in the case of unmodified nanoparticles (Table 1, entry 6).

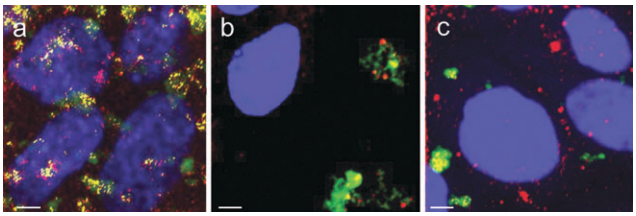

Fig. 6 Co-localisation of red fluorescence emitted by a Cy5-labelled antibody against the early endosomal protein EEA1 and the green fluorescence of Ru@SiO_2 nanoparticles. Nanoparticle-incubated cells were fixed and processed for immunofluorescence microscopy. Single optical sections of the cells incubated for 5 min with (a) unmodified (b) aminopropylated and (c) PEGylated Ru@SiO_2 nanoparticles. Determination of intensity thresholds for the co-localisation has been described earlier,[16] and was monitored by an automatic thresholding device, which made use of an algorithm excluding intensity pairs that exhibit no correlation (Pearson's coefficient < 0). Scale bars are 3 μm. xz and yz views are given in the ESI (see S1).†

However, an increasingly strong fluorescent signal (Fig. 7b and c) inside the cell was obtained in both cases of modified Ru@SiO_2 nanoparticles (Table 1, entries 8 and 10). This suggests that all nanoparticles reached the late endosomal compartment, and that transport to this station is not affected by the surface modification. However, the strong co-localisation of the modified nanoparticles indicates a block to their endocytotic pathway, which could be a consequence of their impaired interaction with the subdomains of late endosomes that control their further delivery to lysosomes. On the contrary, unmodified particles showed no block or time-course hindrance at the late endosomal stage, which supports the minor co-localisation observed in this case (Fig. 7a).

In order to test this hypothesis, we examined the co-localisation of nanoparticles with the lysosomal marker lamp3. Confocal images of MDCK II cells after 60 min incubation with unmodified, aminopropylated and PEGylated Ru@SiO_2 nanoparticles are shown in Fig. 8a–c, respectively. Interestingly, the confocal micrographs showed that after 60 min of incubation, only unmodified Ru@SiO_2 nanoparticles displayed co-localisation with Cy5-Lamp3 (Fig. 8a), whereas modified particles failed to show significant overlap with the lysosomal marker (Fig. 8b and c).

Our data show that, although all the incubated particles are taken up by the cells, only silica particles whose surface carries

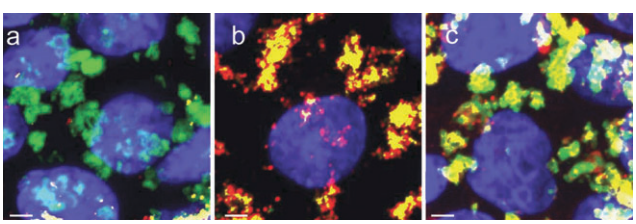

Fig. 7 Co-localisation of Ru@SiO_2 nanoparticles with Cy5-labelled rabbit polyclonal antibodies against late endosomal protein rab7 cell organelles. Single optical sections of the cells visualized after (a) 10 min incubation with unmodified nanoparticles, (b) 30 min incubation with aminopropylated nanoparticles and (c) 30 min incubation with PEGylated Ru@SiO_2 nanoparticles. Scale bars are 3 μm. xz and yz views are given in the ESI (see S2).†

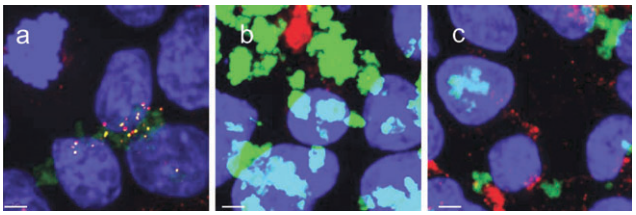

Fig. 8 Co-localisation of $Ru@SiO_2$ nanoparticles with Cy5-labelled rabbit polyclonal antibodies against the lysosomal marker protein lamp3. Single optical sections of the cells visualized after 60 min incubation with (a) unmodified, (b) aminopropylated and (c) PEGylated $Ru@SiO_2$ nanoparticles. Scale bars are 3 μm. xz and yz views are given in the ESI (see S3).†

hydroxyl groups can effectively reach the lysosomes. This is supported by quantitative analysis (Fig. 9), which demonstrates that unmodified nanoparticles are taken up readily by early endosomes and accumulate in lysosomes, after having passed the late endosomal compartment. In contrast, modified particles display less overlap with the early endosomal and lysosomal markers, indicating—at least in part—retention in the late endosomes. This indicates that the chemical character of the functional groups decorating the surface of the particles has a dominant effect on the intercellular fate of the internalized particles, their time course and on the mechanism of their endocytic pathway. We suggest that only the naked silica surface of the unmodified nanoparticles can interact with microdomains in the late endosomal membrane, and are thus translocated, ending up in lysosomes.

It is worth pointing out that a comparison of Rab7 co-localisations with unmodified particles in Fig. 7a and Fig. 9 might show opposed results. However, the two figures cannot be compared directly, because Fig. 7a, which shows only a minor co-localisation, is composed of a singular section, with maximum intensity projections only for a given z axis, whereas Fig. 9 gives percentages of total voxel volume of co-localisation, which may differ widely from that in a projection or a singular section. In Fig. 7, the sections were mainly selected for the best illustration of co-localisation and nuclei.

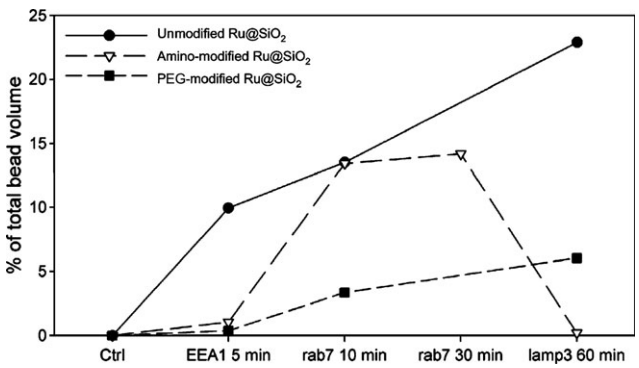

Fig. 9 Quantification of co-localisation between nanoparticles unmodified $Ru@SiO_2$ (●), amino-modified $Ru@SiO_2$ (▽), PEG-modified $Ru@SiO_2$ (■) and various marker proteins for endocytic compartments. The graph plots the percentage of total bead volume against time and the appropriate marker protein (EEA1 = early endosomes, rab7 = late endosomes, lamp3 = lysosomes).

In conclusion, we have prepared spherical silica nanoparticles, with a uniform size ranging from 30 to 200 nm, using a reverse micelle process. The size of the silica nanoparticles could be tuned through control of the water to surfactant ratio. The hydrophilic character of the particles was modulated *via* surface modification, and was shown to have a significant effect on the bulk morphology. Confocal fluorescence microscopy was used to follow the internalization process of $Ru@SiO_2$ nanoparticles inside cultured MDCK II cells. *In vitro* experiments showed that the endocytic pathway of the $Ru@SiO_2$ particles varies with their surface chemistry. All three types of particles tested were taken up by MDCK II cells within 5 min, and all reached the late endosomes after 30 min. However, at this stage, their endocytotic fate was found to be different. While non-functionalised silica particles reached the lysosome compartments after 60 min, no clear evidence of a co-localisation of either aminopropylated or PEGylated nanoparticles was observed.

We conclude that $Ru@SiO_2$ nanoparticles with an average diameter of 200 nm are suitable candidates for following intracellular uptake in living cells, and for studying the effect of the surface chemistry of internalized particles on their endocytotic fate. This will enable us to develop strategies to design target-specific drug delivery systems based on silica nanoparticles, which will provide a better understanding of intracellular delivery mechanisms.

We thank Dr Patrick Shahgaldian, Dr Carla Da Costa and Prof. Venkat Reddy for fruitful discussions and their reading of the manuscript. Ms Céline Pitner, Mr Marcus Waser, Mr Theodor Bühler, Mr Helmut Fally and Mr André Büttler are gratefully acknowledged for FTIR, TGA, DLS and zeta potential experiments. MCDK II cells were kindly supplied by Dr Mattias Wymann, Clinical Department of Biomedicine (DKBW), CH-4058 Basel, Switzerland. This work is supported by the FHNW/HLS research fund.

Experimental

Synthesis of $Ru@SiO_2$ nanoparticles

In a typical experiment, the reverse microemulsion was prepared by mixing Triton X100 (2.92 mM, 2.04 equiv.), n-hexanol (1.43 mM, 1 equiv.) and cyclohexane (69.4 mM, 48.5 equiv.), followed by the addition of 100 μl of an aqueous solution of $[Ru(bpy)_3]Cl_2$ (1.34 mM). The mixture was stirred magnetically for 30 min, after which time TEOS (0.45 mM, 0.32 equiv.) was added, followed by 60 μl of ammonia. After a 24 h reaction, mono-shell silica nanoparticles could be isolated or subsequently surface-modified. For the surface modification of the silica particles, amino groups or PEG groups were introduced directly during the growth of a second silica shell around the core *via* the co-hydrolysis of TEOS and APTES, or TEOS and SPEGS, respectively.

Biospeciation studies

The rabbit antiserum recognizing the tight junction peripheral membrane protein ZO-1 was obtained from Invitrogen-Zymed (LuBioScience GmbH, Lucerne, Switzerland). The mouse monoclonal antibody against the early endosomal protein

EEA1 was purchased from BD Biosciences, Franklin Lakes, NJ, USA. Secondary antibodies of multi-labelling grade and conjugated to Cy5 were purchased from Amersham Pharmacia Biotech or Jackson (La Roche, Switzerland). The rabbit polyclonal antibodies against late endosomal protein rab7 and the lysosomal membrane protein lamp-3 were obtained from Santa Cruz Biotechnology, CA, USA. Confluent monolayers of MDCK cells on microscope cover-slips were analyzed using confocal laser scanning microscopy (LSM 510 Meta, Carl Zeiss, Feldbach, Switzerland) operating in sequential acquisition mode for crosstalk elimination. Image stacks were analyzed for co-localisation with the co-localisation module of the Imaris software package (Bitplane AG, Zurich, Switzerland).

References

1 A. Burns, H. Ow and U. Wiesner, *Chem. Soc. Rev.*, 2006, **35**, 1028; L. M. Liz-Marzan, M. Giersig and P. Mulvaney, *Langmuir*, 1996, **12**, 4329.
2 I. Igor, B. G. Slowing, S. G. Trewyn and V. S.-Y. Lin, *Adv. Funct. Mater.*, 2007, **17**, 1225.
3 S. Santra, D. Dutta and B. M. Moudgil, *Food Bioprod. Process.*, 2005, **83**, 136.
4 F. C. Wang, R. Yuan and Y. Q. Chai, *Appl. Microbiol. Biotechnol.*, 2006, **72**, 671; Y. Liu and H. Jiang, *Electroanalysis*, 2006, **18**, 1007.
5 H. Xu, F. Yan, E. E. Monson and R. Kopelman, *J. Biomed. Mater. Res., Part A*, 2003, **66A**, 870.
6 Y. Chen, H. Y. Chen, D. Zhang and X. H. Xia, *Anal. Bioanal. Chem.*, 2004, **379**, 1025.
7 A. Budny, F. Novak, N. Plumere, B. Schetter, B. Speiser, D. Straub, H. A. Mayer and M. Reginek, *Langmuir*, 2006, **22**, 10605; S. Santra, R. P. Bagwe, D. Dutta, J. T. Stanley, G. A. Walter, W. Tan, B. M. Moudgil and R. A. Mericle, *Adv. Mater.*, 2005, **17**, 2165.
8 P. Ekwall, L. Mandell and K. Fontell, *J. Colloid Interface Sci.*, 1970, **33**, 215.
9 R. P. Bagwe, C. Yang, L. R. Hiliard and W. Tan, *Langmuir*, 2004, **20**, 8336.
10 A. van Blaaderen and A. Vrij, *Langmuir*, 1992, **8**, 2921.
11 H. Neha, P. Radhika, B. Sreedhar and M. Lakshmi Kantan, *J. Nanosci. Nanotechnol.*, 2007, **7**, 3662; S. Santra, P. Zhang, K. Wang, R. Tapec and W. Tan, *Anal. Chem.*, 2001, **73**, 4988.
12 Ch. K. Lim, J.-S. Lee, T. H. Ha, I. Ch. Kwon, Ch.-H. Ahn and S. Y. Park, *J. Photochem. Photobiol., A*, 2007, **188**, 149; D. P. O'Neal, L. R. Hirsch, N. J. Halas, J. D. Payne and J. L. West, *Cancer Lett.*, 2004, **209**, 171.
13 R. H. Webb and C. K. Dorey, in *Handbook of Biological Confocal Microscopy*, ed. J. B. Pawley, Plenum, New York, 2nd edn., 1995, pp. 55.
14 L. Landmann and P. Marbet, *Microsc. Res. Tech.*, 2004, **64**, 103.
15 K. Mostov, T. Su and M. ter Beest, *Nat. Cell Biol.*, 2003, **5**, 287.
16 S. V. Costes, D. Daelemans, E. H. Cho, Z. Dobbin, G. Pavlakis and S. Lockett, *Biophys. J.*, 2004, **86**, 3993.